

Article

Mixed Convection in MHD Water-Based Molybdenum Disulfide-Graphene Oxide Hybrid Nanofluid through an Upright Cylinder with Shape Factor

Yu-Ming Chu ^{1,2}, Kottakkaran Sooppy Nisar ³, Umair Khan ⁴, Hamed Daei Kasmaei ^{5,6}, Manuel Malaver ^{6,7}, Aurang Zaib ⁸ and Ilyas Khan ^{9,*}

¹ Department of Mathematics, Huzhou University, Huzhou 313000, China; chuyuming@zjhu.edu.cn

² Hunan Provincial Key Laboratory of Mathematical Modeling and Analysis in Engineering, Changsha University of Science & Technology, Changsha 410114, China

³ Department of Mathematics, College of Arts and Science, Prince Sattam bin Abdulaziz University, Wadi Al-Dawaser 11991, Saudi Arabia; n.sooppy@psau.edu.sa

⁴ Department of Mathematics and Social Sciences, Sukkur IBA University, Sukkur 65200, Pakistan; umairkhan@iba-suk.edu.pk

⁵ Department of Applied Mathematics, Islamic Azad University-Central Tehran Branch, Tehran 86831-14676, Iran; hamedelectroj@gmail.com

⁶ Bijective Physics Institute, 5280 Idrija, Slovenia; mmf.umc@gmail.com

⁷ Department of Basic Sciences, Maritime University of the Caribbean, Catia la Mar 1162, Venezuela

⁸ Department of Mathematical Sciences, Federal Urdu University of Arts, Science & Technology, Gulshan-e-Iqbal Karachi-75300, Pakistan; aurangzaib@fuuast.edu.pk

⁹ Faculty of Mathematics and Statistics, Ton Duc Thang University, Ho Chi Minh City 72915, Vietnam

* Correspondence: ilyaskhan@tdtu.edu.vn

Received: 11 May 2020; Accepted: 15 June 2020; Published: 17 June 2020



Abstract: In this work, water is captured as regular fluid with suspension of two types of hybrid nanoparticles, namely molybdenumdisulfide (MoS_2) and graphene oxide (GO). The impact of Lorentz's forces on mixed convective boundary-layer flow (BLF) is studied through an upright cylinder under the influences of thermal radiation. The shape factor is also assessed. The mathematical model for hybrid nanofluid is developed and, by implementing suitable similarity variables, the leading partial differential equations (PDEs) are altered into a non-linear ordinary differential equations (ODEs) system and then resolved through a *bvp4c* solver. The penetrations of varied parameters, such as thermal radiation, nanomaterials shapes (bricks, platelets, bricks and cylinders), magneto-hydrodynamics (MHD), and ratio parameters on the temperature and fluid velocity, along with the skin friction and the Nusselt number, are typified qualitatively via sketches. The opposing flow, as well as the assisting flow, is considered. The results indicate that the impact of hybrid nanofluid (HBNF) on the velocity and the temperature is more than nanofluid (NF). It is also scrutinized that the blade-shaped nanomaterials of hybrid nanofluid have a maximum temperature and brick-shaped nanomaterials have a low temperature. In addition, the friction factor and the heat transport rate decline due to the magnetic parameter and increase due to the shape factor. Moreover, the radiation uplifts the velocity and temperature, while the free stream Reynolds number declines the velocity and temperature. Finally, a comparison with available results in the literature are made and found in an excellent way. The ranges of constraints in this research are considered as: $0.01 \leq \lambda \leq 0.2$, $0 \leq M \leq 4$, $0 \leq \alpha \leq 1.5$, $0 \leq R_d \leq 1$, $1 \leq \text{Re}_a \leq 3$, $0 \leq \phi_1 \leq 0.1$ and $0 \leq \phi_2 \leq 0.003$.

Keywords: water; hybrid nanofluid; mixed convection; axisymmetric flow; shape factor; cylinder

1. Introduction

In recent years, nanofluids and their importance have been influenced by many scientists and researchers due to several applications in numerous realistic processes, such as cancer treatment, cooling of electronic devices, the nuclear industry, drug delivery, etc. Nanofluids involve nanomaterials of nanometer-sizes (<100 nm). These are created through the colloidal suspensions of nanomaterials in a regular liquid. Common liquids, such as oils, water, and lubricant fluids, can also be utilized as a regular fluid, similar to polymer solutions and biological fluids. Since the regular fluids have low thermal conductivity. Nanomaterials are utilized to augment the competence in the heat transfer of regular fluids due to the particle formation, which consequently upsurges the thermal conductivity. Several progressions have since been under surveillance by means of nanofluid, having numerous groups.

Very recently, hybrid nanofluid (HBNF) has been used, a class of nanofluids that is devolved through integrating the particular class of nanoparticles inside the functional fluid. Hybrid nanofluids are achieved through suspending two different nanomaterials in the regular fluid. HBNFs are extensively utilized in several fields of engineering, such as cooling of the motors, machining coolant, biomedical, heat pipe reduction in medication, refrigeration, boats by enhanced performance, and space airplanes. Jana et al. [1] experimentally investigated the hybrid nanofluid for the first time in 2007. Sarkar et al. [2] presented a comprehensive and detailed investigation regarding the properties of HBNF. They showed that HBNF significantly augments the pressure, as well as the heat transfer. The field of magnetics on stagnationpoint flow containing water based TiO_2 -Cu hybrid nanofluid through a stretched surface with shape factors was explored by Ghadikolaei et al. [3]. Their studies revealed that the nanoparticles that were platelet-shaped are more effective compared with other shapes. The characteristics of the transfer rate of heat in water-based diamond-cobalt oxide HBNF through an open square cavity was examined by Kalidasan and Kanna [4]. They observed that the heat transfer intensity is greater in the case of the right wall compared to the left wall. Iqbal et al. [5] discussed the impact of water-based SiO_2 nanoparticles and MoS_2 - SiO_2 HBNF from a curved stretched sheet under the impact of heat generation, magnetic field, shape factors, slip effect, and thermal radiation. Their results showed that the flow moves faster in the phenomenon of hybrid nanofluid compared to nanofluid. The significant impact of time-dependent thermal conductivity on non-linear radiated rotated flow, comprising water-based Cu- Al_2O_3 HBNF through a 3D stretched surface, was scrutinized by Usman et al. [6]. Their outcomes designate that suction/injection, porosity, and Hartmann parameters accelerate the surface friction. The stimulus of Lorentz forces on natural convective flow with the features of heat transport, involving hybrid nanofluid with erratic viscosity, was investigated by Manjunatha et al. [7]. The thickness of the boundary-layer of a normal nanofluid, as well as a hybrid nanofluid, moderates owing to the decline in erratic viscosity, whereas temperature and fluid flow of both nanofluids augment with volume fraction. The natural convective flow with heat transport through a rectangular enclosure, comprising a ferroparticle nanotube, was examined by Shi et al. [8]. They utilized an innovative magnetically-controlled technique to augment the performance of the heat transfer. Shi et al. [9] reported that the technique augments heat transfer magnetically by utilizing the magnetic nanoparticles through a straight tube and then compared their results with experimental results. They observed that the efficiency of heat transfer was enhanced up to 12.2% by utilizing the magnetic field. Nawaz and Nazir [10] scrutinized the electrically conducting fluid, comprising ethylene glycol-based Carreau liquid by dispersing the molybdenum disulfide (MoS_2)/ SiO_2 hybrid nanoparticles in ethylene glycol. They reported that the shear stress exerted on the elastic sheet through HBNF is superior to the shear stress exercised via nanofluid (NF). Recently, Shi et al. [11] utilized the Fe_3O_4 magnetic particles to establish the speedy heat conduction between the heat sink and heat source through a channel. At 30 mT, the Nusselt number in the lack of magnetic field has an enrichment of 112.4%, while the stable temperature declines via 22.6% by magnetic Fe_3O_4 nanofluid by utilizing a magnetic number.

The exploration of magneto-hydrodynamics (MHD) procedures for awareness on fluid through nanofluids has now developed to be very applicable and operational in several sectors of engineering, sciences, and technology. Applications include wound treatments, generators based on MHD power, optical modulators, and many more. Additionally, this field's theoretical analysis conveys knowledge about the Lorentz forces. This group of force is created owing to the MHD impact, which is an extremely supportive argument to control the structure of cooling. In this view, the principles of the law of Maxwell and Ohm are highly beneficial. The latest concepts regarding this area can be studied in References [12–15]. Hayat et al. [16] focused on the related research in this field. Their results indicated that the temperature of fluid increases due to thermophoresis and Brownian motion. The impact of a MHD-comprising nanofluid is explored by Lin et al. [17]. Four changed kinds of nanoparticles, namely CuO, Cu, TiO₂, and Al₂O₃, along with temperature dependent viscosity, are discussed. Haq et al. [18] investigated the MHD influences on squeezing flow, involving water-based metallic nanomaterials. They confirmed that the copper nanoparticle gives superior heat transfer compared to other mixtures. Recently, Khan et al. [19] examined the non-linear radiation impact on MHD flow, containing titanium alloy nanomaterials in the direction of stream wise and cross flow with activation energy, and found the dual outcomes for a certain number of moving parameters.

As stated above, the current survey is crowded with many works containing the characteristics of heat transfer comprising non-Newtonian and Newtonian fluids. On the other hand, the research regarding the mixed convection flows with heat transfer, involving hybrid nanofluid, has revealed to be realistically significant in engineering processes, for example, cooling and heating processes in electrical devices, car radiators (engine cooling systems), nuclear reactors, solar collectors, heat exchangers, etc. However, the review of literature illustrated that mixed convection flow through an upright cylinder embedded in the hybrid nanofluid was not taken into account. In addition, this analysis comprises a novel era for scientists to discover the thermal and hydrodynamic features of magnetic hybrid nanofluids. Thus, in this paper, the central aim is the inspection of the Lorentz's forces on mixed convective boundary-layer flow, involving water-based MoS₂-GO hybrid nanofluid through an upright cylinder under the influences of thermal radiation and its shape factor. The similarity procedure is used to discover the result of transmuting differential equations through a bvp4c solver. The graphical results are elaborated in detail.

2. Formulation of the Problem

Consider a steadily mixed convective axisymmetric stagnation point flow through an upright stretching cylinder, as shown in Figure 1. The shape factor, radiation, and magnetic fields are taken into account in this perusal. The cylinder surface is in contact by involving MoS₂-graphene oxide (GO) hybrid nanofluids in a water-based fluid. The cylinder is expressed by $r = a$ in the polar cylindrical coordinate. The flow is axisymmetric, regarding the z -axis, and is also symmetric at the $z = 0$ plane. The ambient fluid had an invariable temperature T_∞ and the cylinder is preserved at a temperature $T = T_w$. $T_w < T_\infty$ signifies the opposing flow, while $T_w > T_\infty$ indicates the assisting flow. The gravitational acceleration g proceeds in the downhill direction. A magnetic function is pertained in the r -direction. Let z and r be the cylindrical polar-coordinate distances measuring in the axial and the radial directions, respectively. It is presumed that hybrid nanofluid is subject to the fixed magnetic field B_0 . Additionally, the induced magnetic field (IMF) is ignored owing to the tiny magneto Reynolds number. There are two key physical impacts that arise when liquids shift into a magnetic field. The electric field \mathbf{E} is the first effect, which is induced in the fluid flow. It is assumed that the charge density has no access and, thus, $\nabla \times \mathbf{E} = 0$. Ignoring the IMF signifies that $\nabla \times \mathbf{E} = 0$, thus neglecting the induced electric field. The second influence is enthusiastic in nature, i.e., Lorentz force ($\mathbf{J} \times \mathbf{B}$) with \mathbf{J} represents the current density. This type of force operates on the liquid and adapts fluid motion. In the current exploration, the relativistic influences are ignored, and \mathbf{J} is defined through Ohm's law: $\mathbf{J} = \sigma(\mathbf{V} \times \mathbf{B})$.

The governing equations of hybrid nanofluid involving MHD are expressed as [20]:

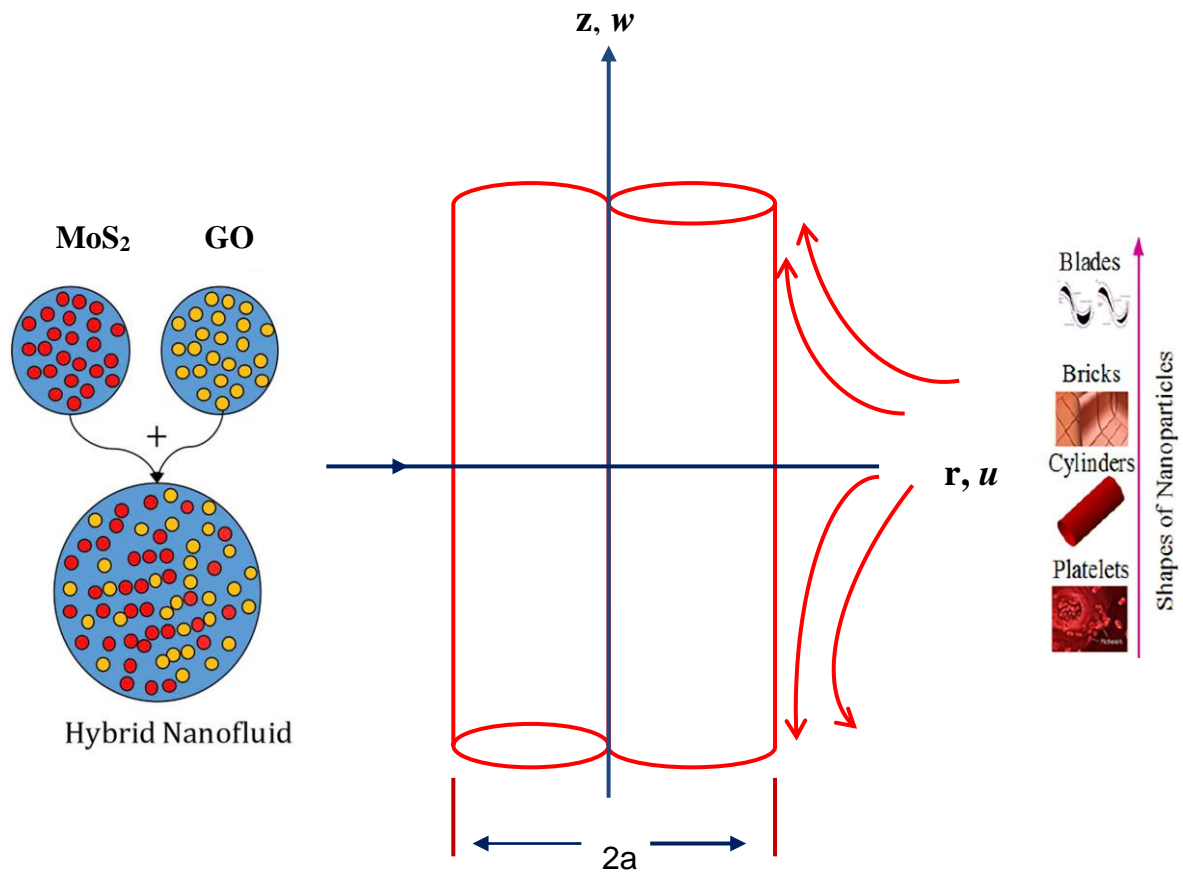


Figure 1. Diagram of the problem [3].

$$\frac{\partial(ru)}{\partial r} + r \frac{\partial w}{\partial z} = 0 \tag{1}$$

$$w \frac{\partial u}{\partial z} + u \frac{\partial u}{\partial r} = -\frac{1}{\rho_{hbnf}} \frac{\partial p}{\partial r} + \nu_{hbnf} \left(\frac{\partial^2 u}{\partial r^2} + \frac{1}{r} \frac{\partial u}{\partial r} - \frac{u}{r^2} \right) - \frac{\sigma_{hbnf} B_0^2}{\rho_{hbnf}} u \tag{2}$$

$$w \frac{\partial w}{\partial z} + u \frac{\partial w}{\partial r} = -\frac{1}{\rho_{hbnf}} \frac{\partial p}{\partial z} + \nu_{hbnf} \left(\frac{\partial^2 w}{\partial r^2} + \frac{1}{r} \frac{\partial w}{\partial r} \right) - \frac{\sigma_{hbnf} B_0^2}{\rho_{hbnf}} w \pm g \frac{(\rho\beta)_{hbnf}}{\rho_{hbnf}} (T - T_\infty) \tag{3}$$

$$u \frac{\partial T}{\partial r} + w \frac{\partial T}{\partial z} = \frac{k_{hbnf}}{(\rho c_p)_{hbnf}} \left(\frac{\partial^2 T}{\partial r^2} + \frac{1}{r} \frac{\partial T}{\partial r} \right) - \frac{1}{(\rho c_p)_{hbnf}} \frac{1}{r} \frac{\partial}{\partial r} (r q_r) \tag{4}$$

The subjected appropriate boundary conditions comprise the permeable boundary, velocity, and variable temperature at the surface of the cylinder, in which A and A_1 are the respective cylinder twist rate and the constant linear rate, while, mathematically, the velocities for a cylinder at the free surface or the far field of the stagnation flow of strain rate B and the radius of cylinder a , along with the ambient temperature, are written as:

$$\begin{aligned} u = 0, w = 2Az, T = T_w = T_\infty + A_1 z \text{ at } r = a, \\ u = -B\left(r - \frac{a^2}{r}\right), w = 2Bz, T \rightarrow T_\infty \text{ as } r \rightarrow \infty. \end{aligned} \tag{5}$$

where u and w are the coordinate velocities in the corresponding directions of r and z , while p is the pressure and $\beta_{hbnf}, \nu_{hbnf}, \rho_{hbnf}, \sigma_{hbnf}, (\rho c_p)_{hbnf}, k_{hbnf}$ symbolize the thermal expansion coefficient, kinematic viscosity, density, electrical conductivity, heat capacity, and thermal conductivity of the HBNFs, respectively. The final term in Equation (3) signifies the effect of buoyancy force, which has

positive and negative signs, where the positive sign indicates the buoyancy assisting flow, while a negative sign indicates the buoyancy opposing flow. Moreover, in the energy Equation (4), q_r is the radiative heat flux, which is expressed through the approximation of the Rosseland:

$$q_r = -\frac{16\sigma^*T_\infty^3}{3k^*} \frac{\partial T}{\partial r} \tag{6}$$

where k^* signifies the mean constant of absorption and σ^* indicates the constant of Stefan Boltzmann.

Here, we endeavored to attempt a novel method to alter the mode of heat transfer in fluids that are freshly examined among researchers. We utilized the hybrid nanomaterials, together with the varied structures of nanomaterials and base fluids, which is estimated to be a proficient path to modifying the procedure of the transport rate of heat in fluids. Therefore, the attributes of the thermophysical features of regular liquid and hybrid nanofluids are specified in Table 1, with the thermophysical features of the regular liquid and nanomaterials that are suggested in Table 2. Meanwhile, Table 3 shows the different shape effects m .

We introduced the following similarity transformations:

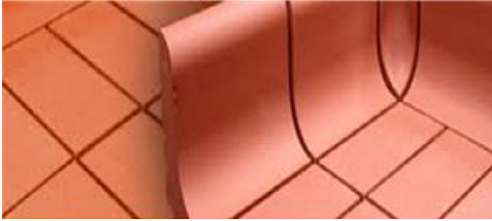
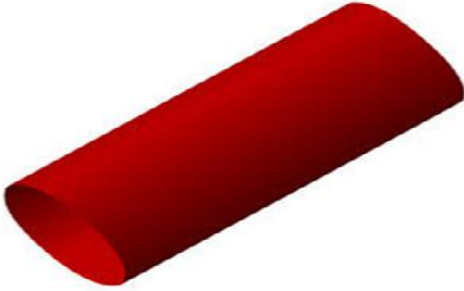
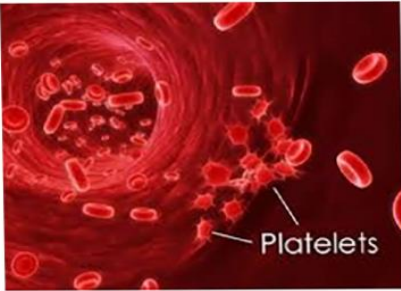
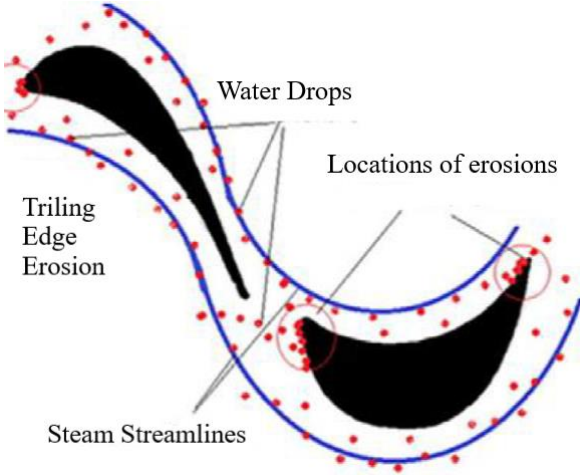
Table 1. Thermophysical elements of hybrid nanofluid and regular fluid [10,21].

Properties	Nanofluid	Hybrid Nanofluid
Density	$\rho_{nf} = \{(1-\phi)\rho_f + \phi\rho_s\}$	$\rho_{hbnf} = [(1-\phi_2)\{(1-\phi_1)\rho_f + \phi_1\rho_{s_1}\} + \phi_2\rho_{s_2}]$
Viscosity	$\mu_{nf} = \frac{\mu_f}{(1-\phi)^{2.5}}$	$\mu_{hbnf} = \frac{\mu_f}{(1-\phi_1)^{2.5}(1-\phi_2)^{2.5}}$
Thermal expansion	$(\rho\beta)_{nf} = [(1-\phi)(\rho\beta)_f + \phi(\rho\beta)_s]$	$(\rho\beta)_{hbnf} = (1-\phi_2)[(1-\phi_1)(\rho\beta)_f + \phi_1(\rho\beta)_{s_1}] + \phi_2(\rho\beta)_{s_2}$
Electrical conductivity	$\sigma_{nf} = \sigma_f \left[1 + \frac{3(\sigma-1)\phi}{(\sigma+2)-(\sigma-1)\phi} \right]$	$\sigma_{hbnf} = \sigma_{bf} \left[\frac{\sigma_{s_2}(1+2\phi_2)+2\sigma_{bf}(1-\phi_2)}{\sigma_{s_2}(1-\phi_2)+\sigma_{bf}(2+\phi_2)} \right]$ with $\sigma_{bf} = \sigma_f \left[\frac{\sigma_{s_1}(1+2\phi_1)+2\sigma_f(1-\phi_1)}{\sigma_{s_1}(1-\phi_1)+\sigma_f(2+\phi_1)} \right]$
Thermal conductivity	$\frac{k_{nt}}{k_f} = \frac{k_s+(m-1)k_t-(m-1)\phi(k_f-k_s)}{k_s+(m-1)k_t+\phi(k_f-k_s)}$	$\frac{k_{hbnf}}{k_f} = \frac{k_{s_2}+(m-1)k_{bf}-(m-1)\phi_2(k_{bf}-k_{s_2})}{(k_{s_2}+2k_{nt})+\phi_2(k_{nf}-k_{s_2})}$ with $k_{bf} = \frac{k_{s_1}+(m-1)k_f-(m-1)\phi_1(k_f-k_{s_1})}{k_{s_1}+(m-1)k_f-\phi_1(k_f-k_{s_1})} \times k_f$
Heat capacity	$(\rho c_p)_{nf} = [(1-\phi)(\rho c_p)_f + \phi(\rho c_p)_s]$	$(\rho c_p)_{hbnf} = (1-\phi_2)[(1-\phi_1)(\rho c_p)_f + \phi_1(\rho c_p)_{s_1}] + \phi_2(\rho c_p)_{s_2}$

Table 2. Thermo physical properties of the base fluid and hybrid nanoparticles [3].

Characteristic Properties	H ₂ O	MoS ₂	GO
ρ	997.1	5060	1800
c_p	4179	397.21	717
k	0.613	904.4	5000
σ	0.005	2.09×10^4	6.30×10^7
β	21	2.8424×10^{-5}	2.84×10^{-4}
Pr	6.2	-	-

Table 3. Shapes of the nanoparticle with their values.

Nanoparticle Type	Shape	Shape Factor
Bricks		3.7
Cylinders		4.9
Platelets		5.7
Blades		8.6

$$u = -Aa \frac{f(\xi)}{\sqrt{\xi}}, w = 2Azf'(\xi), \xi = \left(\frac{r}{a}\right)^2, \theta(\xi) = \frac{T - T_\infty}{T_w - T_\infty}. \tag{7}$$

When implementing the transformations above into Equations (2) to (5) and obtaining consistent transmutordinary differential equations (ODEs) via the well-known Equation (7), we get:

$$g_1(\xi f''' + f'') + g_2 Re_a(\alpha^2 + ff'' - (f')^2) + g_3 Re_a M(\alpha - f') + g_4 \lambda Re_a \theta = 0 \tag{8}$$

$$(\xi\theta'' + \theta')\left[g_5 + \frac{4}{3}R_d\right] + g_6\text{Re}_a\text{Pr}(f\theta' - f'\theta) = 0 \tag{9}$$

The subjected major boundary restriction is:

$$\begin{aligned} f(1) = 0, f'(1) = 1, \theta(1) - 1 = 0, \\ f'(\infty) \rightarrow \alpha, \theta(\infty) \rightarrow 0. \end{aligned} \tag{10}$$

in which:

$$\begin{aligned} g_1 &= \frac{1}{(1-\phi_1)^{2.5}(1-\phi_2)^{2.5}}, \\ g_2 &= \left((1-\phi_2)\left\{ (1-\phi_1) + \phi_1 \frac{\rho_{s1}}{\rho_f} \right\} + \phi_2 \frac{\rho_{s2}}{\rho_f} \right), \\ g_3 &= \left(\left[\frac{\sigma_{s2}(1+2\phi_2)+2\sigma_{bf}(1-\phi_2)}{\sigma_{s2}(1-\phi_2)+\sigma_{bf}(2+\phi_2)} \right] \right) \left(\frac{\sigma_{s1}(1+2\phi_1)+2\sigma_f(1-\phi_1)}{\sigma_{s1}(1-\phi_1)+\sigma_f(2+\phi_1)} \right), \\ g_4 &= \left((1-\phi_2)\left[(1-\phi_1) + \phi_1 \frac{(\rho\beta)_{s1}}{(\rho\beta)_f} \right] + \phi_2 \frac{(\rho\beta)_{s2}}{(\rho\beta)_f} \right), \\ g_5 &= \left\{ \frac{k_{s2}-k_{nf}(1-m)+\phi_2(1-m)(k_{nf}-k_{s2})}{k_{s2}-k_{nf}(1-m)+\phi_2(k_{nf}-k_{s2})} \right\} \left\{ \frac{k_{s1}-k_f(1-m)+\phi_1(1-m)(k_f-k_{s1})}{k_{s1}-k_f(1-m)+\phi_1(k_f-k_{s1})} \right\}, \\ g_6 &= \left((1-\phi_2)\left[\phi_1 \frac{(\rho c_p)_{s1}}{(\rho c_p)_f} + (1-\phi_1) \right] + \phi_2 \frac{(\rho c_p)_{s2}}{(\rho c_p)_f} \right), \end{aligned} \tag{11}$$

The non-dimensional constraints in Equations (8)–(10) are mathematically expressed as:

$$\begin{aligned} \lambda = \frac{Gr_z}{\text{Re}_z^2}, M = \frac{\sigma_f B_0^2}{2\rho_f A}, \text{Re}_z = \frac{Az^2}{2\nu_f}, \text{Pr} = \frac{\nu_f}{\alpha_f}, Gr_z = \frac{g\beta_f(T_w-T_\infty)z^3}{16\nu_f^2}, \text{Re}_a = \frac{Aa^2}{2\nu_f}, \alpha = \frac{B}{A}, \\ R_d = \frac{4\sigma^* T_\infty^3}{k_f k^*}. \end{aligned}$$

Whilst also presenting the above-mentioned constraints with their names, the problem is clearly exercised and signified in the mixed convective (λ) parameter (which is defined as $\lambda = Gr_z/\text{Re}_z^2$ and called the fraction of Grashof number (Gr_z) and the Reynolds number (Re_z), the magnetic parameter (M), Prandtl number (Pr), free stream Reynolds number (Re_a), velocity ratio parameter (α) and the (R_d) radiation parameter).

The local heat transport rate, or the Nusselt number and the friction factor, are considerable quantities regarding the flow through heat transfer. These quantities in the form of ODEs are:

$$Nu_z = \frac{-k_{hbnf}z}{k_f(T_w - T_\infty)} \left(\frac{\partial T}{\partial r} \right)_{r=a} \tag{12}$$

$$C_{fz} = \frac{\mu_{hbnf}}{\frac{1}{2}\rho w^2} \left(\frac{\partial w}{\partial r} \right)_{r=a}, w = 2Az \tag{13}$$

Applying (7) to (12) and (13), we get:

$$\frac{1}{2} \left(\frac{\text{Re}_z}{\text{Re}_a} \right)^{-\frac{1}{2}} Nu_z = \frac{-k_{hbnf}}{k_f} \theta'(1) \tag{14}$$

$$\sqrt{\text{Re}_z \text{Re}_a} C_{fz} = \frac{f''(1)}{(1-\phi_1)^{2.5}(1-\phi_2)^{2.5}} \tag{15}$$

3. Results and Discussions

The nonlinear ODEs (8) and (9), with restricted conditions (10), were numerically exercised via bvp4c, based on the Lobatto IIIA formula. Table 4 is prepared for validation of the current result $f''(1)$, with published outcomes of Fang et al. [22] and Hamid et al. [23] in the restrictive cases, who found an excellent agreement. The outcomes of diverse constraints in the existence of shape factors of

nanoparticles on fluid velocity and temperature profile, along with friction factor and the Nusselt number for nanofluids, as well as hybrid nanofluid phases, have been examined through the graphs (Figures 2–15) and tabulated in Tables (Tables 5 and 6). Additionally, the assisting flow and opposing flow were discussed.

Table 4. Comparison of the current result [$f''(1)$] with the existing result in a steady flow case when $M = \alpha = Re_a = R_d = \lambda = \phi_1 = \phi_2 = 0$.

Current Result	Fang et al. [22]	Hamid et al. [23]
−1.1778	−1.17775	−1.17776

Figures 2 and 3 inspect the influence of mixed parameter λ on the profiles of velocity and temperature, respectively. It is clear from Figure 2 that the velocity of fluid is more pronounced for greater λ in the case of assisting flow. Physically, the greater amount of λ generated a larger buoyancy force, which gave the highest moving energy, and such energy generates the confrontation through the flow. The contrary trend was analyzed for the velocity in the case of opposing flow. Figure 3 reveals that the temperature and the corresponding boundary layer declined due to λ in the assisting and opposing flows. Figures 4 and 5 depict the impact of magnetic parameter on the velocity and temperature profiles. Figure 4 indicates that the magnetic parameter resisted with the velocity of fluid in the hybrid nanofluid, as well as the nanofluid and, as an output, the velocity boundary-layer thickness declined. Physically, the existence of the magnetic field engendered the Lorentz forces, which were, in fact, the drag force. The flow and Lorentz force acted in a contrary way to each other, which caused the flow retardation. Figure 5 explains that by amplifying the potency of magnetic parameter, the fluid temperature augmented. Physically, a resistive kind of force, such as the Lorentz force, countered with the fluid motion, thus heat was fabricated, and, consequently, the temperature and corresponding boundary-layer thickness was thicker. In addition, it is clear from these profiles that the fluid flow accelerated more for hybrid nanoparticles as compared to MoS₂/water nanoparticles. Figures 6 and 7 highlight the impact of radiation parameter on the fluid velocity and temperature distribution. It is transparent from these portraits that the fluid motion and temperature distribution augmented due to the magnifying of the radiation parameter. Physically, the surface of the heat flux increased due to the radiation, and, consequently, a higher temperature in the boundary-layer flow (BLF) region should be approximated. The achieved result was a confirmation of the legitimacy of the relation R_d . Additionally, the radiation was utilized to collapse the molecules of water into hydrogen. The influences of shape factors on the temperature distribution and velocity are portrayed in Figures 8 and 9, respectively. The velocity and temperature of the HBNF is also shown, as well as a nanofluid augment with the shape factor. Physically, the sturdy hydrogen bonding of HBNF and NF caused a sharp augment in the thermal conductivity and thus the velocity and temperature profiles enhanced. In addition, the temperature was at a maximum for the blade shape and at a minimum in the case of the cylinder for hybrid nanofluid and for nanofluid. Figures 10 and 11 demonstrate the inspiration of Re_a on the temperature and velocity fields for hybrid nanofluid and nanofluid. It is expected from these profiles that the velocity and temperature decline with escalating values of Re_a . The stimulus of the nanoparticle volume fraction ϕ_2 on the velocity and temperature profiles are portrayed in Figures 12 and 13 for the assisting and opposing flows. Figure 12 explains that the velocity augments with ϕ_2 for $\lambda > 0$ and declines for $\lambda < 0$. The upsurge in the velocity is owing to the reality that the dynamic viscosity of hybrid nanofluid had an inverse relation with the volume fraction. Therefore, an augment in ϕ_2 guided to decline the viscosity of regular fluid and consequently accelerated the fluid flow. Whereas, the contrary impact was seen on the temperature (Figure 13). The patterns of streamlines with and without hybrid nanofluid are portrayed in Figures 14 and 15. Major deviation in the trajectories was seen among the particle motion.

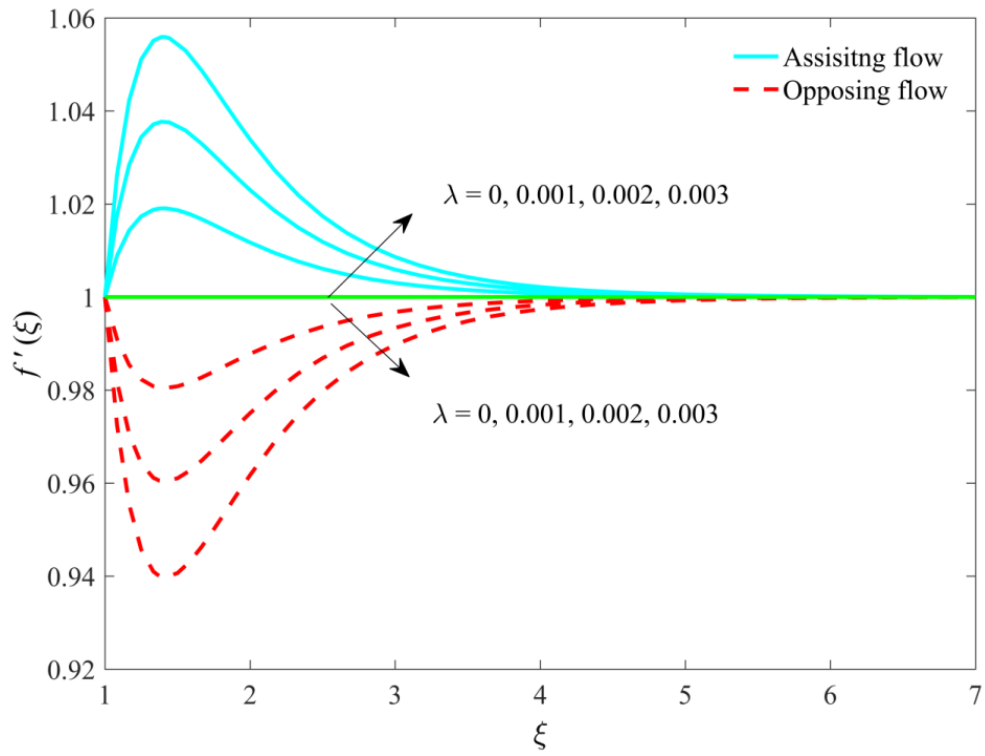


Figure 2. Impact of λ on $f'(\xi)$.

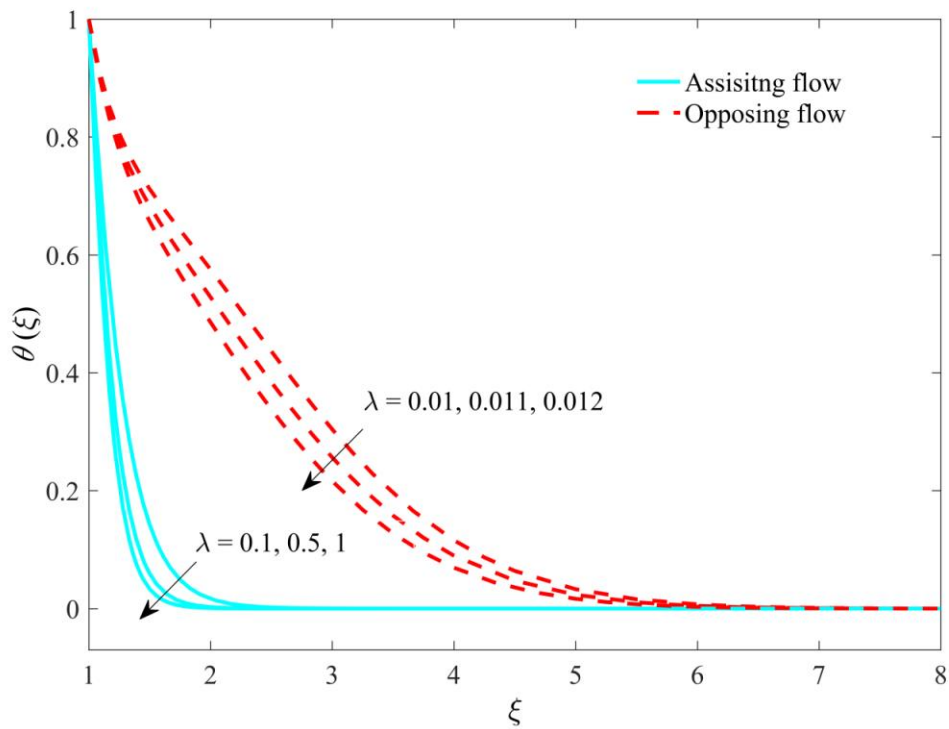


Figure 3. Impact of λ on $\theta(\xi)$.

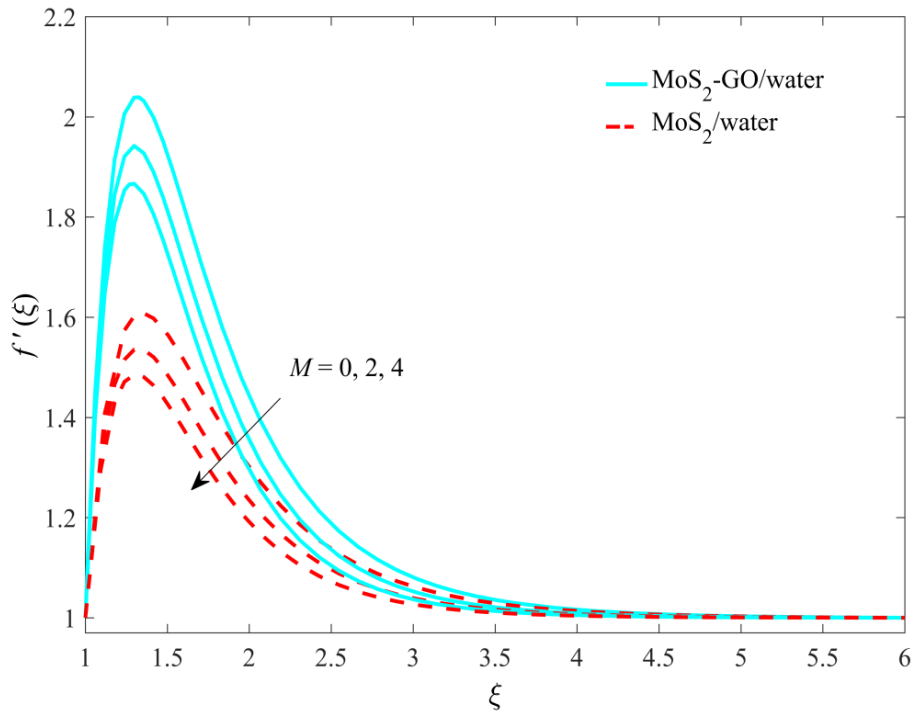


Figure 4. Impact of M on $f'(\xi)$.

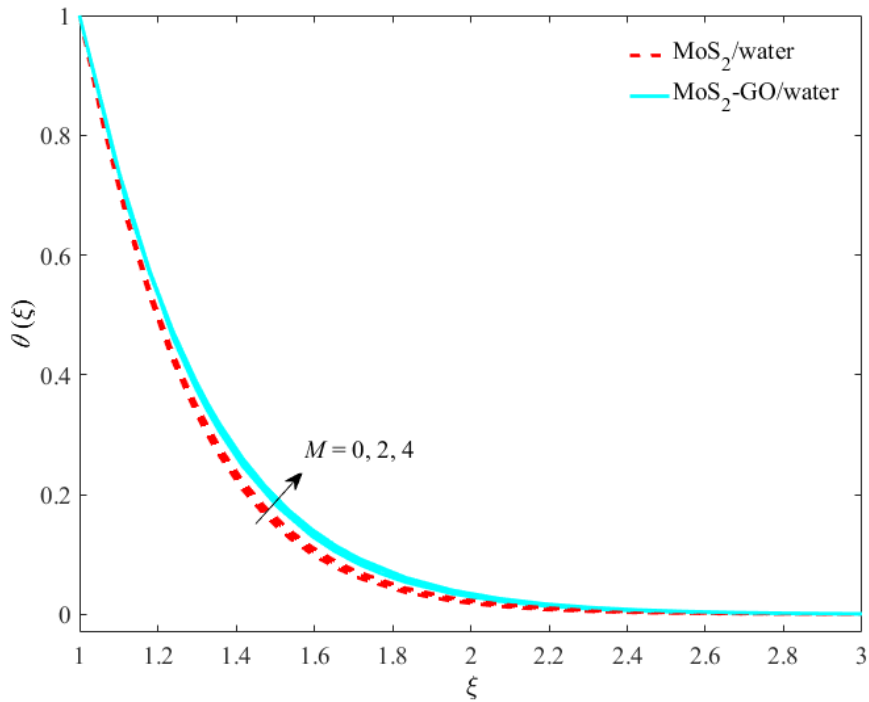


Figure 5. Impact of M on $\theta(\xi)$.

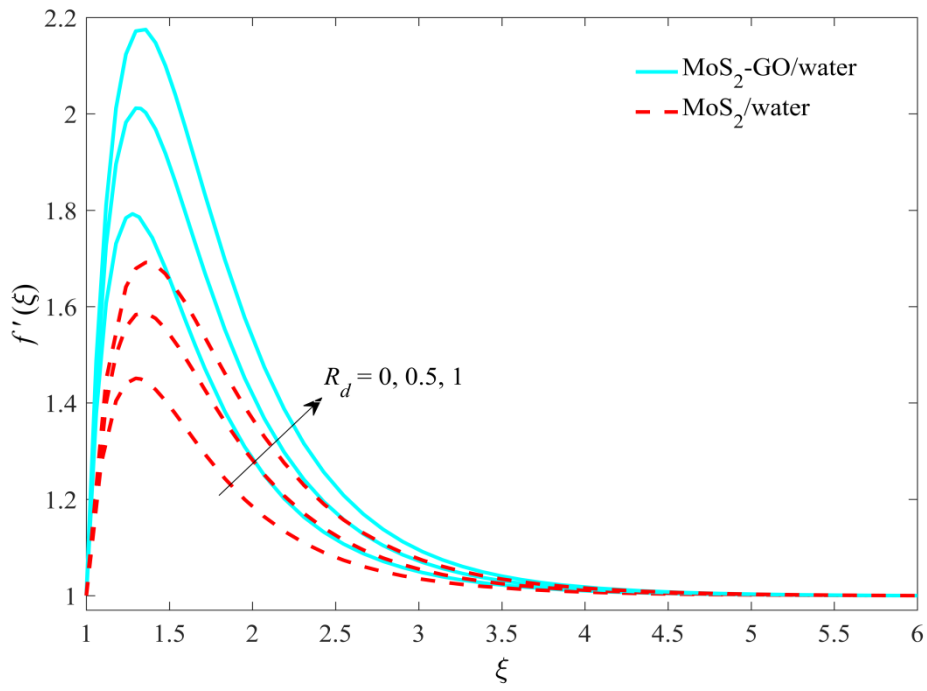


Figure 6. Impact of R_d on $f'(\xi)$.

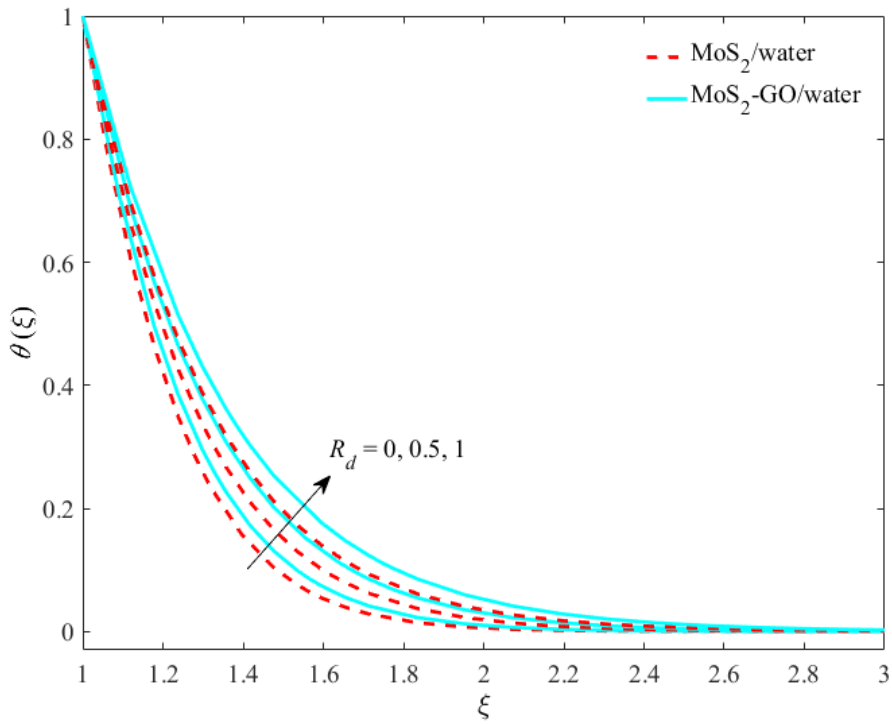


Figure 7. Impact of R_d on $\theta(\xi)$.

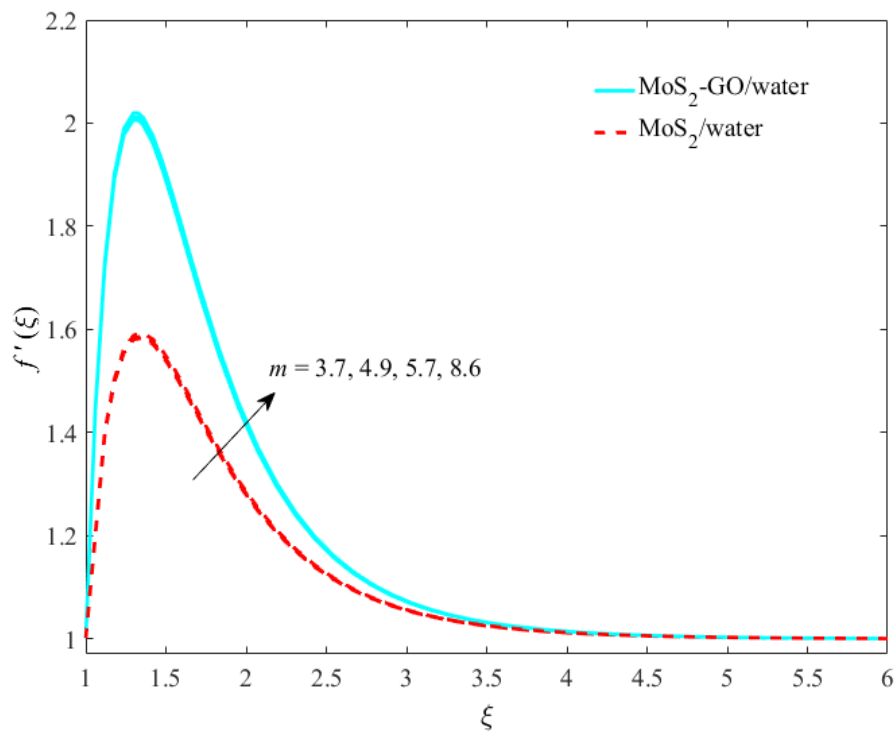


Figure 8. Impact of m on $f'(\xi)$.

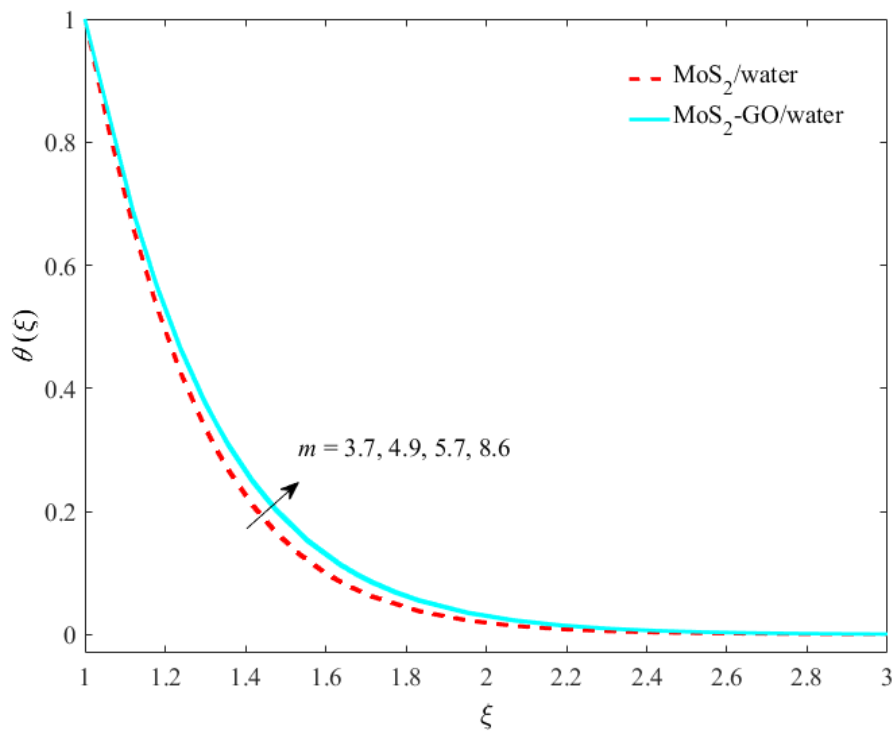


Figure 9. Impact of m on $\theta(\xi)$.

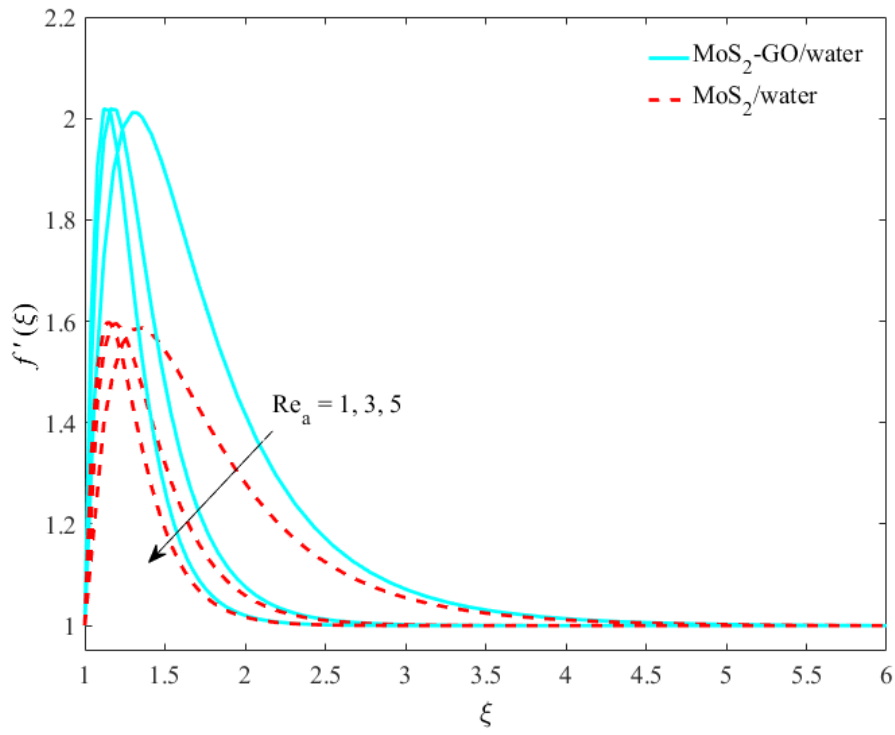


Figure 10. Impact of Re_a on $f'(\xi)$.

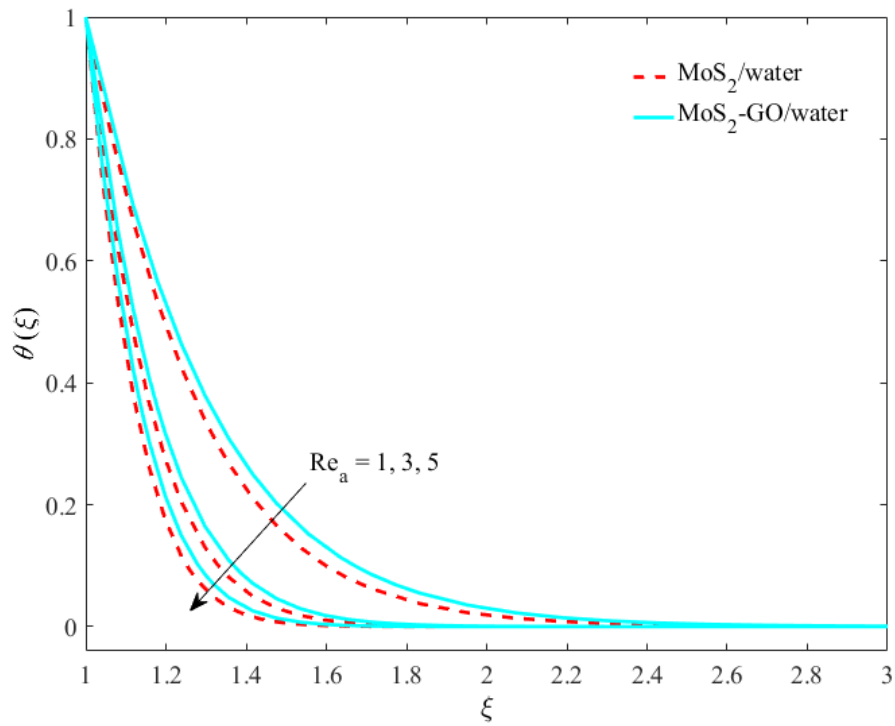


Figure 11. Impact of Re_a on $\theta(\xi)$.

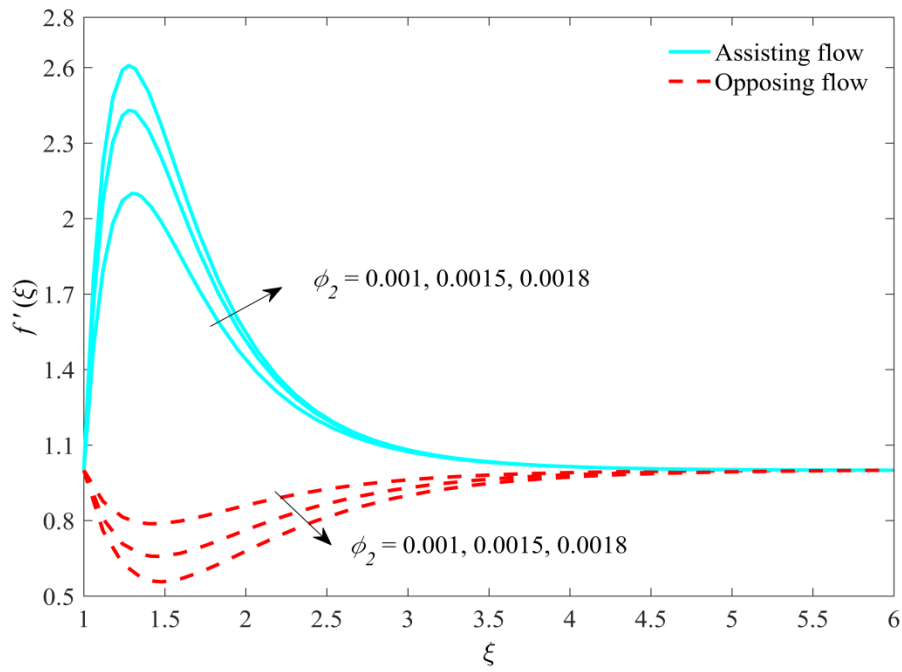


Figure 12. Impact of ϕ_2 on $f'(\xi)$.

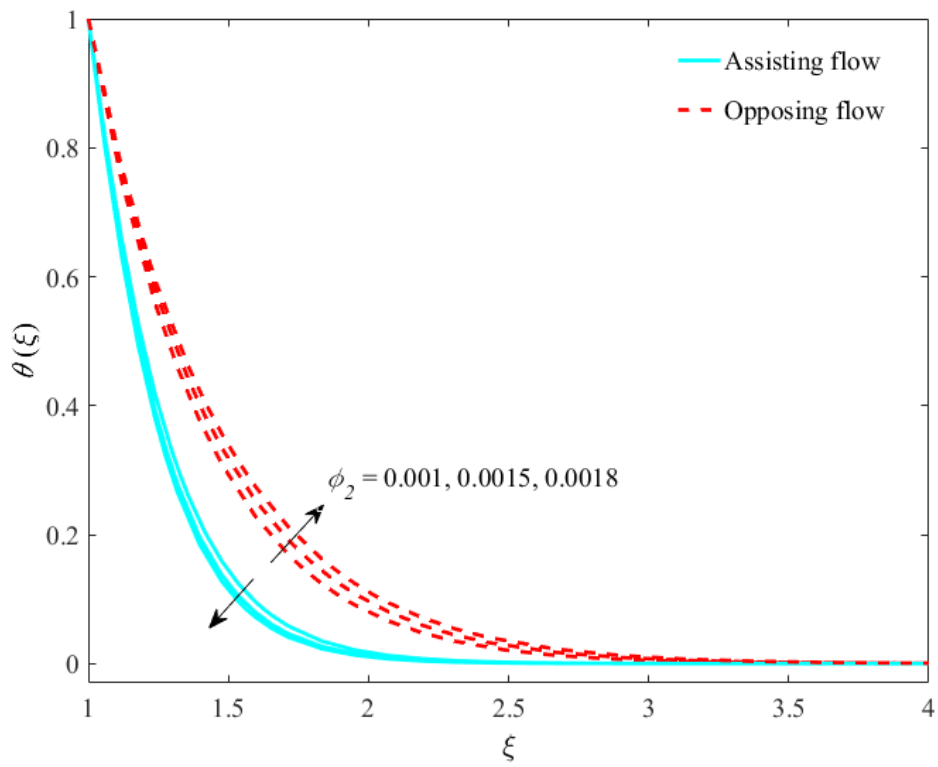


Figure 13. Impact of ϕ_2 on $\theta(\xi)$.

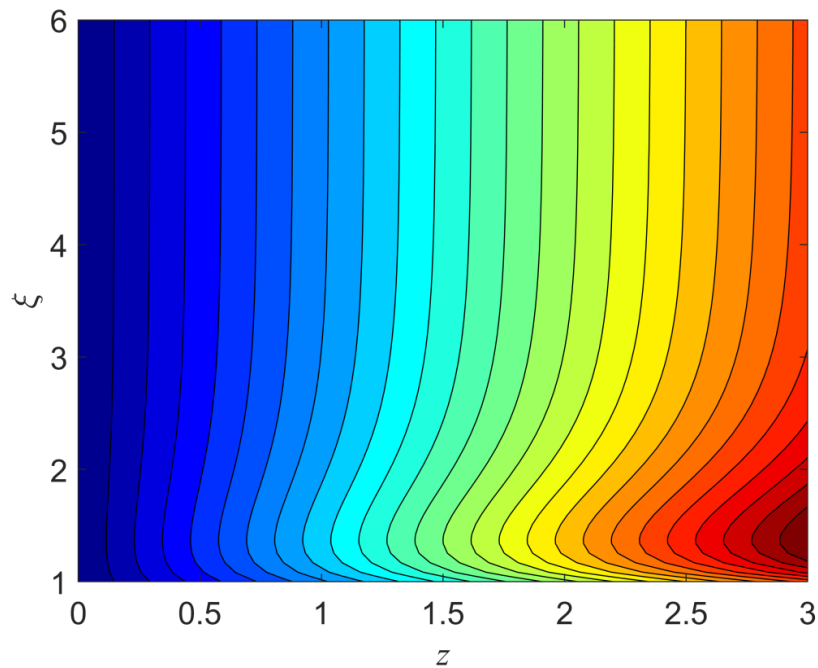


Figure 14. Streamline patterns for normal nanofluid.

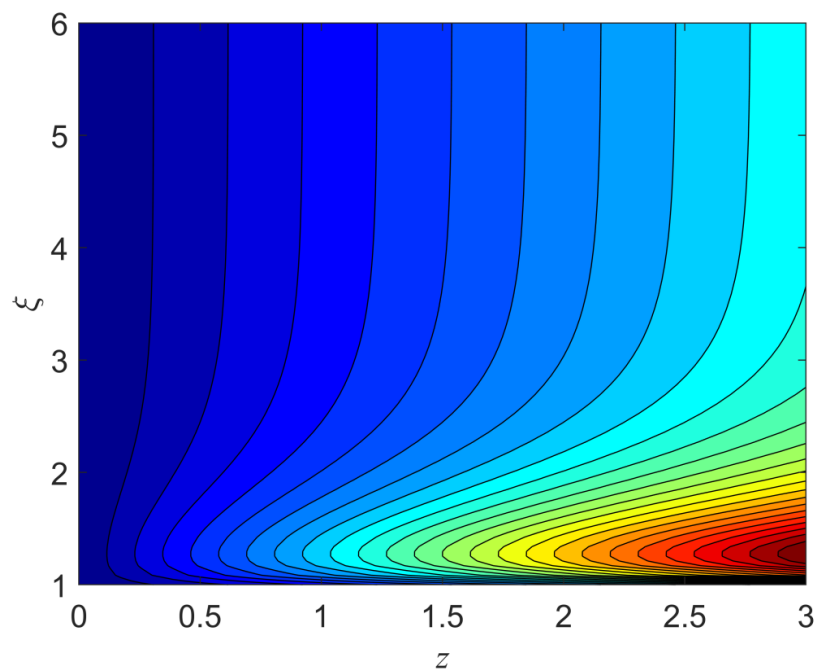


Figure 15. Streamline patterns for hybrid nanofluid.

Tables 5 and 6 were prepared to see the influence of volume fraction ϕ_1 and magnetic parameter M on the skin factor and the rate of heat transport for hybrid nanofluid with different shape factors, respectively. In Table 5, it is apparent that for $m = 3.7, 4.9, 5.7,$ and 8.6 , enhancements of 9.082%, 9.126%, 9.154%, and 9.62%, respectively, are observed in the friction factor in case of hybrid nanofluid, while there were enhancements of 18.925%, 18.972%, 18.997%, and 19.111%, respectively, in the normal nanofluid. Alternatively, for $m = 3.7, 4.9, 5.7,$ and 8.6 , the heat transport rate augmented by 1.024%, 1.192%, 1.300%, and 1.682%, respectively, in case of hybrid nanofluid, whereas it augmented by 1.148%, 1.317%, 1.425%, and 1.805% in the case of normal nanofluid with ϕ_1 . Physically, the thermal conductivity was enhanced due to ϕ_1 , which consequently boosted up the transfer rate of heat in both

nanofluids. In addition, the skin factor and the heat transport rate were greater in the case of blade shape and were lower in the cylinder shape. Whereas, the skin factor and the heat transport rate declined due to magnetic function for hybrid nanofluid, as well as for normal nanofluid, as shown in Table 6. Table 6 guarantees 2.539%, 2.551%, 2.547%, and 2.559% and 2.247%, 2.249%, 2.256%, and 2.267% reduction in the skin friction for normal and hybrid nanofluids for $m = 3.7, 4.9, 5.7,$ and $8.6,$ respectively. Whereas, the heat transfer shrank up to 0.159%, 0.160%, 0.161%, and 0.164% and 0.246%, 0.248%, 0.249%, and 0.254%, respectively, for normal and hybrid nanofluids.

Table 5. Impact of nanoparticle fraction ϕ_1 on $\sqrt{Re_z Re_a} C_{fz}$ and $(1/2)(Re_z/Re_a)^{-\frac{1}{2}} Nu_z$ for molybdenum disulfide (MoS₂)\water and MoS₂-GO/water when $M = 0.5, \alpha = 1, Re_a = 1, R_d = 0.5, \lambda = 0.1, \phi_2 = 0.00001.$

Quantities	ϕ_1	3.7		4.9		5.7		8.6	
		Nano	Hybrid	Nano	Hybrid	Nano	Hybrid	Nano	Hybrid
$\sqrt{Re_z Re_a} C_{fz}$	0.01	1.1091	2.1922	1.1116	2.1969	1.1133	2.2000	1.1192	2.2111
	0.012	1.3190	2.3913	1.3225	2.3974	1.3248	2.4014	1.3331	2.4157
	0.014	1.5269	2.5892	1.5316	2.5968	1.5347	2.6018	1.5457	2.6197
$\frac{1}{2} \left(\frac{Re_z}{Re_a} \right)^{-\frac{1}{2}} Nu_z$	0.01	2.8222	2.9181	2.8462	2.9433	2.8622	2.9601	2.9195	3.0202
	0.012	2.8546	2.9480	2.8837	2.9784	2.9030	2.9986	2.9722	3.0710
	0.014	2.8866	2.9775	2.9208	3.0132	2.9435	3.0369	3.0246	3.1217

Table 6. Impact of magnetic parameter M on $\sqrt{Re_z Re_a} C_{fz}$ and $(1/2)(Re_z/Re_a)^{-\frac{1}{2}} Nu_z$ for MoS₂\water and MoS₂-GO/water when $\phi = 0.01, \alpha = 1, Re_a = 1, R_d = 0.5, \lambda = 0.1, \phi_2 = 0.00001.$

Quantities	M	3.7		4.9		5.7		8.6	
		Nano	hybrid	Nano	hybrid	Nano	hybrid	Nano	hybrid
$\sqrt{Re_z Re_a} C_{fz}$	0.0	1.1380	2.2426	1.1407	2.2475	1.1424	2.2508	1.1486	2.2624
	0.5	1.1091	2.1922	1.1116	2.1969	1.1133	2.2000	1.1192	2.2111
	1.0	1.0832	2.1464	1.0856	2.1509	1.0871	2.1539	1.0928	2.1645
$\frac{1}{2} \left(\frac{Re_z}{Re_a} \right)^{-\frac{1}{2}} Nu_z$	0.0	2.8267	2.9253	2.8508	2.9507	2.8668	2.9675	2.9243	3.0279
	0.5	2.8222	2.9181	2.8462	2.9433	2.8622	2.9601	2.9195	3.0202
	1.0	2.8181	2.9115	2.8421	2.9367	2.8581	2.9534	2.9152	3.0133

4. Conclusions

In this perusal, the mixed convective magneto flow, with heat transport containing MoS₂-GO/water hybrid nanofluids near a stagnation point through a vertical stretched cylinder with shape factors and radiation impacts, was explored. The similarity technique was used to alter the partial differential equations (PDEs) into nonlinear ODEs, and these transmuted PDEs were worked out through a bvp4c solver. The fluid velocity upsurges and declines were due to $\lambda,$ respectively, in the assisting flow and opposing flow. Meanwhile, the temperature distribution shrank in the assisting and opposing flows. However, the magnetic number uplifted the temperature and decelerated the velocity, along with the Nusselt number and the skin friction for hybrid nanofluid and normal nanofluid. The radiation and shape factor significantly enhanced the velocity and temperature, as well as the skin factor and the Nusselt number. The velocity increased due to ϕ_2 in the assisting flow and decelerated in the opposing flow, while the contrary impact was perceived on the temperature profile.

Author Contributions: Conceptualization, A.Z. and U.K.; methodology, I.K.; software, U.K.; validation, U.K., M.M. and H.D.K.; formal analysis, K.S.N.; investigation, U.K.; resources, Y.-M.C.; data curation, A.Z.; writing—original draft preparation, K.S.N.; writing—review and editing, Y.-M.C.; visualization, I.K.; supervision, M.M.; project administration, K.S.N.; funding acquisition, Y.-M.C. All authors have read and agreed to the published version of the manuscript.

Funding: This project was supported by the Natural Science Foundation of China (Grant Nos. 61673169, 11701176, 11626101, 11601485).

Acknowledgments: The authors would like to acknowledge the financial support of the Natural Science Foundation of China (Grant Nos. 61673169, 11701176, 11626101, 11601485).

Conflicts of Interest: The authors declare no conflict of interest.

Nomenclature

A, A_1, B	cylinder twist, linear, and strain rate
a	radius of cylinder
B_0	magnetic field intensity ($\text{kg/s}^2 \text{ A}$)
C_{fz}	skin friction coefficient
c_p	specific heat (J/kg K)
g	gravity acceleration (m s^{-2})
Gr_z	Grashof number
k^*	mean absorption coefficient
k_{hbnf}	thermal conductivity of the hybrid nanofluid ($\text{W m}^{-1} \text{ K}^{-1}$)
k_{nf}	thermal conductivity of the nanofluid ($\text{W m}^{-1} \text{ K}^{-1}$)
k_{s1}	thermal conductivity of nanoparticles ($\text{W m}^{-1} \text{ K}^{-1}$)
M	Hartmann number
m	shape factor
Nu_z	Nusselt number
Pr	Prandtl number
p	the pressure
q_r	radiative heat flux
R_d	radiation parameter
Re_z	local Reynolds number
Re_a	free stream Reynolds number
T	temperature (K)
T_∞	free-stream temperature (K)
T_w	wall temperature (K)
(u, w)	velocity components (m s^{-1})
(r, z)	Cartesian coordinates (m)

Greek symbols

α	velocity ratio parameter
β_{hbnf}	hybrid nanofluid thermal expansion (K^{-1})
β_f	base fluid thermal expansion (K^{-1})
β_{s1}, β_{s2}	nanoparticle thermal expansion (K^{-1})
λ	mixed convective parameter
μ_{hbnf}	hybrid nanofluid dynamic viscosity (kg m s^{-1})
μ_f	base fluid dynamic viscosity (kg m s^{-1})
ϕ_1, ϕ_2	volume fraction of nanoparticles
θ	dimensionless temperature
ν_{hbnf}	kinematic viscosity of hybrid nanofluid ($\text{m}^2 \text{ s}^{-1}$)
ρ_{hbnf}	hybrid nanofluid density (kg m^{-3})
ρ_s	nanoparticles density (kg m^{-3})
ρ_f	density of base fluid (kg m^{-3})
$(\rho c_p)_{hbnf}$	heat capacity of the hybrid nanofluids
σ^*	Stefan Boltzmann constant
σ_{hbnf}	electrical conductivity of hybrid nanofluid (s/m)
ψ	stream function
ξ	similarity variable

Subscripts

f	condition at free stream
s	solid nanoparticles
nf	nanofluid
$hbnf$	hybrid nanofluid
w	wall boundary condition
∞	free-stream condition

Superscripts

'	derivative w.r.t. ξ
---	-------------------------

References

- Jana, S.; Salehi-Khojin, A.; Zhong, W.H. Enhancement of fluid thermal conductivity by the addition of single and hybrid nano-additives. *Thermochim. Acta.* **2007**, *462*, 45–55. [[CrossRef](#)]
- Sarkar, J.; Ghosh, P.; Adil, A. A review on hybrid nanofluids: Recent research, development and applications. *Renew. Sustain. Energy Rev.* **2015**, *43*, 164–177. [[CrossRef](#)]
- Ghadikolaei, S.S.; Yassari, M.; Sadeghi, H.; Hosseinzadeh, K.; Ganji, D.D. Investigation on thermophysical properties of TiO₂-Cu/H₂O hybrid nanofluid transport dependent on shape factor in MHD stagnation point flow. *Powder Technol.* **2017**, *322*, 428–438. [[CrossRef](#)]
- Kalidasan, K.; Kanna, P.R. Natural convection on an open square cavity containing diagonally placed heaters and adiabatic square block and filled with hybrid nanofluid of nanodiamond-cobalt oxide/water. *Int. Commun. Heat Mass Transf.* **2017**, *81*, 64–71. [[CrossRef](#)]
- Iqbal, Z.; Maraj, E.N.; Azhar, E.; Mehmood, Z. A novel development of hybrid (MoS₂-SiO₂/H₂O) nanofluidic curvilinear transport and consequences for effectiveness of shape factors. *J. Taiwan Inst. Chem. Eng.* **2017**, *81*, 150–158. [[CrossRef](#)]
- Usman, M.; Hamid, M.; Zubair, T.; Haq, R.U.; Wang, W. Cu-Al₂O₃/Water hybrid nanofluid through a permeable surface in the presence of nonlinear radiation and variable thermal conductivity via LSM. *Int. J. Heat Mass Transf.* **2018**, *126*, 1347–1356. [[CrossRef](#)]
- Manjunatha, S.; Kuttan, B.A.; Jayanthi, S.; Chamkha, A.; Gireesha, B.J. Heat transfer enhancement in the boundary layer flow of hybrid nanofluids due to variable viscosity and natural convection. *Heliyon* **2019**, *5*, e01469. [[CrossRef](#)]
- Shi, L.; He, Y.; Hu, Y.; Wang, X. Thermophysical properties of Fe₃O₄@CNT nanofluid and controllable heat transfer performance under magnetic field. *Energy Conver. Manag.* **2018**, *177*, 249–257. [[CrossRef](#)]
- Shi, L.; Hu, Y.; He, Y. Magnetocontrollable convective heat transfer of nanofluid through a straight tube. *Appl. Thermal Eng.* **2019**, *162*, 114220. [[CrossRef](#)]
- Nawaz, M.; Nazir, U. An enhancement in thermal performance of partially ionized fluid due to hybrid nano-structures exposed to magnetic field. *AIP Adv.* **2019**, *9*, 085024. [[CrossRef](#)]
- Shi, L.; Hu, Y.; He, Y. Magneto-responsive thermal switch for remote-controlled locomotion and heat transfer based on magnetic nanofluid. *Nano Energy* **2020**, *71*, 104582. [[CrossRef](#)]
- Khan, M.; Hashim, A. A revised model to analyze the heat and mass transfer mechanisms in the flow of Carreaunanofluids. *Int. J. Heat Mass Transf.* **2016**, *103*, 291–297.
- Zaib, A.; Rashidi, M.M.; Chamkha, A.J.; Bhattacharyya, K. Numerical solution of second law analysis for MHD Cassonnanofluid past a wedge with activation energy and binary chemical reaction. *Int. J. Num. Meth. Heat Fluid Flow* **2017**, *27*, 2816–2834.
- Raza, J.; Mebarek-Oudina, F.; Mahanthesh, B. Magnetohydrodynamic flow of nano Williamson fluid generated by stretching plate with multiple slips. *Multidiscip. Mod. Mat. Struct.* **2019**, *15*, 871–894. [[CrossRef](#)]
- Shateyi, S.; Tendayi, G. Numerical analysis of unsteady MHD flow near a stagnation point of a two-dimensional porous body with heat and mass transfer, thermal radiation, chemical reaction. *Boundary Val. Prob.* **2014**, *5*, 218. [[CrossRef](#)]
- Hayat, T.; Muhammad, T.; Qayyum, A.; Alseadi, A.; Mustafa, M. On squeezing flow of nanofluid in the presence of magnetic field effects. *J. Mol. Liq.* **2016**, *213*, 179–185. [[CrossRef](#)]

17. Lin, Y.; Zhang, L.; Zhang, X.; Ma, L.; Chen, G. MHD pseudo-plastic nanofluid unsteady flow and heat transfer on the finite thin film on a stretching surface internal heat generation. *Int. J. Heat Mass Transf.* **2015**, *84*, 903–911. [[CrossRef](#)]
18. Haq, R.; Nadeem, S.; Khan, Z.H.; Noor, N. MHD squeezed flow of water functionalized metallic nanoparticles over a sensor surface. *Physica E* **2015**, *73*, 45–53. [[CrossRef](#)]
19. Khan, U.; Zaib, A.; Khan, I.; Nisar, K.S. Activation energy on MHD flow of titanium alloy (Ti6Al4V) nanoparticle along with a cross flow and streamwise direction with binary chemical reaction and non-linear radiation: Dual Solutions. *J. Mater. Res. Technol.* **2020**, *9*, 188–199. [[CrossRef](#)]
20. Gorla, R.S.R. Mixed convection in an axisymmetric stagnation point flow on a vertical cylinder. *Acta Mech.* **1993**, *99*, 113–123. [[CrossRef](#)]
21. Khashiie, N.S.; Arifin, N.M.; Nazar, R.; Hafizuddin, E.H.; Wahi, N.; Pop, I. Magnetohydrodynamics (MHD) axisymmetric flow and heat transfer of a hybrid nanofluid past a radially permeable stretching/shrinking sheet with Joule heating. *Chin. J. Phys.* **2020**, *64*, 251–263. [[CrossRef](#)]
22. Fang, T.; Zhang, J.; Zhong, Y.; Tao, H. Unsteady viscous flow over an expanding stretching cylinder. *Chin. Phys. Lett.* **2011**, *12*, 124707. [[CrossRef](#)]
23. Hamid, A.; Hashim; Alghamdi, M.; Khan, M.; Alshomrani, A.S. An investigation of thermal and solutal stratification effects on mixed convection flow and heat transfer of Williamson nanofluid. *J. Mol. Liq.* **2019**, *284*, 307–315. [[CrossRef](#)]



© 2020 by the authors. Licensee MDPI, Basel, Switzerland. This article is an open access article distributed under the terms and conditions of the Creative Commons Attribution (CC BY) license (<http://creativecommons.org/licenses/by/4.0/>).